Vibrio harveyi NADPH−FMN Oxidoreductase Arg203 as a Critical Residue for NADPH Recognition and Binding[†]

He Wang,[‡] Benfang Lei,[‡,§] and Shiao-Chun Tu*[,‡,||]

Departments of Biology and Biochemistry and Chemistry, University of Houston, Houston, Texas 77204-5513

Received February 17, 2000; Revised Manuscript Received April 28, 2000

ABSTRACT: Luminous bacteria contain three types of NAD(P)H−FMN oxidoreductases (flavin reductases) with different pyridine nucleotide specificities. Among them, the NADPH-specific flavin reductase from *Vibrio harveyi* exhibits a uniquely high preference for NADPH. In comparing the substrate specificity, crystal structure, and primary sequence of this flavin reductase with other structurally related proteins, we hypothesize that the conserved Arg203 residue of this reductase is critical to the specific recognition of NADPH. The mutation of this residue to an alanine resulted in only small changes in the binding and reduction potential of the FMN cofactor, the K_m for the FMN substrate, and the k_{cat}. In contrast, the K_m for NADPH was increased 36-fold by such a mutation. The characteristic perturbation of the FMN cofactor absorption spectrum upon $NADP^+$ binding by the wild-type reductase was abolished by the same mutation. While the $k_{cat}/K_{m,NADPH}$ was reduced from 1990×10^5 to 46×10^5 M^{-1} min^{-1} by the mutation, the mutated variant showed a $k_{cat}/K_{m,NADH}$ of 4×10^5 M^{-1} min^{-1}, closely resembling that of the wild-type reductase. The deuterium isotope effects ^DV and $^D(V/K)$ for (4*R*)-[4-^{2}H]-NADPH were 1.7 and 1.4, respectively, for the wild-type reductase but were increased to 3.8 and 4.0, respectively, for the mutated variant. Such a finding indicates that the rates of NADPH and $NADP^+$ dissociation in relation to the isotope-sensitive redox steps were both increased as a result of the mutation. These results all provide support to the critical role of the Arg203 in the specific recognition and binding of NADPH.

In recent years the important functional roles of NAD(P)H[1]: flavin oxidoreductases (or flavin reductases) in supplying reduced flavins required by various biological activities have begun to gain recognition (ref *1* and relevant references therein). However, at present, much remains to be explored regarding the structure−function relationships of flavin reductases and very little has been documented with respect to the mechanisms of reduced flavin transfer from flavin reductases to receptor enzymes. Three types of flavin reductases have been identified in luminous bacteria (*2*−*5*). We have proposed to name them flavin reductase P (FRP) for the NADPH-preferring species, flavin reductase D (FRD) for the NADH-preferring species, and flavin reductase G (FRG) for the enzyme that utilizes NADH and NADPH without any marked difference in efficiency (*6*). It is believed that the reduced riboflavin 5′-phosphate ($FMNH_2$) required by luciferase as a substrate for bioluminescence is supplied by at least one of these flavin reductases through direct transfer (*2*, *3*, *5*, *7*). Using *Vibrio harveyi* luciferase and FRP (*6*) as a model system for biological intermolecular transfer of reduced flavin, members of our laboratory have conducted extensive enzymological studies on luciferase and, more recently, have also begun to delineate the structure and mechanism of FRP.

The *frp* gene encoding the *V. harveyi* FRP has been cloned, sequenced, and expressed (*6*). Homogeneous FRP holoenzyme, which binds one FMN cofactor per 26 300-Da monomer (*6*), and apoenzyme (*8*) have been obtained and their structural and catalytic properties have been characterized. Active FRP holoenzyme can be reconstituted from the apoenzyme and both forms undergo a monomer−dimer equilibrium (*8*). FRP has also been crystallized as a homodimer, and its structure was determined without (*9*) and with (*10*) a bound NAD^+ inhibitor. On the basis of kinetic evidence, we found that the *V. harveyi* luciferase indeed acquires $FMNH_2$ from FRP via a direct transfer mechanism (*1*). In addition to the FMN cofactor, FRP also binds FMN as a substrate. The $FMNH_2$ provided by FRP to luciferase could conceivably be either the reduced flavin cofactor or the reduced flavin product of FRP. Interestingly, we found that luciferase preferentially utilizes the reduced FMN cofactor rather than the $FMNH_2$ product of FRP for the coupled bioluminescence reaction (*1*). However, the molecular basis for the preferential transfer of the reduced flavin cofactor of FRP to luciferase and that for the high specificity

[†] Supported by Grants GM25953 from the National Institutes of Health and E-1030 from The Robert A. Welch Foundation.

* Corresponding author: telephone 713-743-8359; fax 713-743-8351; e-mail dtu@uh.edu.

[‡] Department of Biology and Biochemistry.

[§] Present address: Laboratory of Human Bacterial Pathogenesis, Rocky Mountain Laboratories, National Institute of Allergy and Infectious Diseases, National Institutes of Health, 903 S. Fourth St., Hamilton, MT 59840.

[||] Department of Chemistry.

[1] Abbreviations: NADH, nicotinamide adenine dinucleotide, reduced form; NADPH, nicotinamide adenine dinucleotide phosphate, reduced form; FRP, NADPH-preferring flavin reductase; FRD, NADH-preferring flavin reductase; FRG, general flavin reductase that utilizes NADH and NADPH with similar efficiencies; $FMNH_2$, reduced riboflavin 5′-phosphate; q, quantum; IPTG, isopropyl 1-thio-β-D-galactoside; PS, phenosafranin; NADPD, (4*R*)-[4-^{2}H]nicotinamide adenine dinucleotide phosphate (reduced).

10.1021/bi0003745 CCC: $19.00
Published on Web 06/07/2000

of FRP for NADPH remain unclear. The latter was targeted as the focus for the present investigation.

Although the structure of the FRP−NAD^+ complex has been determined, the mode of the NADPH substrate binding must be distinct from that of the NAD^+ inhibitor binding. The NAD^+ bound by FRP is the most folded, with well-defined intramolecular ring stacking, in comparison with that bound to any other proteins for which the crystal structures are known. Moreover, although the bound NAD^+ is right next to the FMN cofactor, the nicotinamide ring is not close to the flavin isoalloxazine ring. In contrast, the functionally active conformation of NADPH requires a close proximity between the nicotinamide and the isoalloxazine for a hydride transfer. Nevertheless, the FRP−NAD^+ structure provides a clue as to how FRP achieves a specificity for NADPH and how it facilitates the release of the $NADP^+$ product (*10*). NADPH and $NADP^+$ are hypothesized to shuttle between an open and a folded conformation during FRP catalysis. It is also proposed that NADPH in an open conformation is the active form for hydride transfer and the closed conformation of $NADP^+$, similar to that of the bound NAD^+, is ready for release as a product. Using 4-^{3}H- and 4-^{2}H-labeled NADPH, we have identified that the 4*R* H of NADPH is transferred to the *re* face of the FRP FMN cofactor (*11*). On the basis of this stereochemical relationship, the proposed open configuration of bound NADPH, the necessary close proximity between the NADPH nicotinamide ring and the flavin isoalloxazine ring, and the FRP crystal structure (*9*), we have identified a potential NADPH site by computer ligand docking using the Quanta program (H. Wang and S.-C. Tu, unpublished results). FRP has a 9-residue (residues A_{201}-S-R-T-S-N-G-K-L_{209}) loop that is not resolved in the crystal structure (*9*). Our ligand docking exercise showed that this loop was very close to the proposed NADPH site. Especially, the Arg203 residue within this loop appeared to be a likely site for interacting with the adenosine 2′-phosphate moiety of NADPH. In this study, we employed the approach of site-directed mutagenesis to investigate the possible functional role of the FRP Arg203 residue in NADPH recognition and binding. Results indeed support such a working hypothesis.

EXPERIMENTAL PROCEDURES

Materials. NADPH, $NADP^+$, NADH, FMN, $NADP^+$-dependent alcohol dehydrogenase from *Thermoanaerobium brockii*, aldehyde dehydrogenase from bakers' yeast, ethanol-d_6, and *N*-tris(hydroxymethyl)methyl-3-aminopropanesulfonic acid (Taps) were all from Sigma. Restriction endonucleases, T4 DNA ligases, and T4 DNA polymerase were from Promega. *Escherichia coli* BL21 and expression vector pET-21d were from Novagen. DEAE-cellulose DE52 was from Whatman. DEAE-Sepharose Fast Flow and phenyl-Sepharose Fast Flow were from Amersham−Pharmacia. All primers were synthesized by Biosynthesis Inc. All phosphate (P_i) buffers were at pH 7.0 and consisted of phosphates at mole fractions of 0.39 sodium monobase and 0.61 potassium dibase.

Site-Directed Mutagenesis. The DNA of pFRP1 (*6*) was digested with *Eco*RI and *Sal*I and the fragment containing the *frp* gene was inserted into M13mp18 at the *Eco*RI and *Sal*I sites. The single-stranded DNA of the resulting construct was used as the template for site-directed mutagenesis. The mutagenesis was carried out by using the Muta-Gene M13 in vitro mutagenesis kit from Bio-Rad and the primer 5′-GATTGCTTGTAGCGCTCGCATAATACG-3′. The sequence is for the antisense strand. The underlined bases were those altered to change the arginine residue at position 203 to an alanine to create the FRP variant R203A. The mutation was verified by DNA sequencing.

Expression of the Wild-Type and Mutated frp Genes. Wild-type and mutant *frp* genes were expressed by use of pET and *E. coli* BL21 system (*12*). The wild-type and mutant *frp* genes were amplified by polymerase chain reaction with the primers 5′-TTATGGTGAGGATCCAGCCAAATA-3′ and 5′-ATATGATGTGAGCTCAACAAAGTG-3′. The underlined bases were those mutated to create the *Bam*HI and *Sac*I restriction enzyme sites. The wild-type and mutant *frp* amplified products were digested with *Bam*HI and *Sac*I and inserted into pET-21d at the same sites to yield pFRP2 and $pFRP^{203A}$, respectively. The insertions were further confirmed by DNA sequencing. The pFRP2- or $pFRP^{203A}$-transformed *E. coli* BL21 cells were first grown at 37 °C overnight in 50 mL of Luria−Bertani medium containing 100 mg/L ampicillin and then transferred to 4 L of the same medium for further growth at the same temperature. Isopropyl 1-thio-β-D-galactoside (IPTG) was added to 0.2 mM when OD_{600} reached about 1.0. Cells were harvested after 4 h of additional growth.

Purification of the Wild-Type and Mutant FRP. Both FRP and R203A were purified by batch adsorption, anion exchange chromatography, and hydrophobic chromatography. About 30 g of cell paste was resuspended in 300 mL of 50 mM P_i containing 0.5 mM dithiothreitol and sonicated on ice for 20 min. The lysed cells were centrifuged for 20 min at 10000*g*. To the supernatant, 15 mL bed volume of DEAE-cellulose DE-52 was added and stirred for 20 min on ice. The resin was washed by 50 mM P_i until the eluate was clear. Active reductase was then recovered by elution with 300 mM P_i. The sample obtained was diluted 6-fold with water and loaded on a 1.5 × 25 cm DEAE-Sepharose column equilibrated with 50 mM P_i. The column was isocratically eluted with 160 mM P_i. The fractions containing active reductase were pooled. The pool was adjusted to 0.8 M ammonium sulfate and was applied to a phenyl-Sepharose column (1.5 × 15 cm) preequilibrated with 1 M ammonium sulfate. The column was washed with 0.8 M $(NH_4)_2SO_4$ in 50 mM P_i until A_{280} reached baseline and then eluted with 0.6 M $(NH_4)_2SO_4$ in 50 mM P_i. The fractions with $A_{453}/A_{273} \geq 0.3$ were pooled and concentrated in the following way. The sample was adjusted to 1 M $(NH_4)_2SO_4$ and loaded on a 1.5 × 5 cm phenyl-Sepharose column. Active reductase was recovered by elution with 50 mM P_i. The enzyme samples so obtained were >90% pure on the basis of sodium dodecyl sulfate−polyacrylamide gel electrophoresis.

Stoichiometry and K_d for the Binding of Cofactor FMN. Apoenzyme of R203A was prepared following procedures reported previously (*8*) and was titrated with various concentrations of FMN. The degrees of quenching of the protein fluorescence at 330 nm were followed by use of 280 nm excitation light, and the stoichiometry and dissociation constants for the cofactor FMN binding were determined as described previously (*8*).

Enzyme Assay. Reductase activities were measured spectrophotometrically (*6*) at 23 °C with FMN and NAD(P)H at designated concentrations. The initial rate was determined as micromoles of NADPH (ϵ_{340} 6.22 mM^{-1} cm^{-1}) oxidized per liter per minute.

Kinetic Isotope Effects. The kinetic isotope effects were determined by measuring the reductase activities with 55 μM FMN and NADPH or (4*R*)-[4-^{2}H]NADPH. (4*R*)-[4-^{2}H]NADPH (NADPD) was synthesized following the procedure of Sem and Kasper (*13*). The crude product was applied to a DE-52 column (1 × 15 cm) preequilibrated with 60 mM sodium phosphate (pH 7.5). The column was first washed with 120 mM sodium phosphate (pH 7.5) and then with 250 mM sodium phosphate (pH 7.5). The fractions with $A_{260}/A_{340} < 2.41$ were collected and used immediately for kinetic isotope effect experiments.

Determination of Redox Potentials. The redox potentials of FRP and R203A were determined at 23 °C by anaerobic spectrophotometric titration (*14*) with NADH. The anaerobic reaction solution (1 mL of 50 mM P_i) initially contained 2 μM benzyl viologen, 20 μM reductase, and 20 μM phenosafranin. The spectrum at equilibrium was taken after each addition of NADH on a Milton Roy 3000 spectrophotometer. Spectral data were analyzed according to the Nernst equation.

RESULTS

Overexpression of FRP and R203A. The *frp* and *frp*^{R203A} genes were expressed under the control of the T7 promoter in *E. coli* BL21 which has the IPTG-inducible gene to encode the T7 RNA polymerase (*12*). The IPTG-induced cells were found to contain FRP or R203A at levels of more than 20% of the total cellular proteins. The levels of expression were much higher than those of the original construct pFRP1 (*6*). The purified FRP and R203A contained one FMN cofactor per enzyme monomer as reported previously, indicating that the high level of expression did not lead to any significant accumulation of apoenzyme. Moreover, the overexpressed FRP was essentially identical to the native FRP from *V. harveyi* with respect to specific activity and general kinetic parameters.

FMN Cofactor Binding by R203A. When 1 μM R203A apoenzyme was titrated with various levels of FMN, changes in the protein fluorescence intensities were measured and plotted against the molar ratio of [FMN]/[enzyme monomer] (Figure 1). The maximal fluorescence change was found to be at a molar ratio of 0.9, indicating that the mutant enzyme binds one FMN per monomer. In another fluorescence titration experiment, a limiting level of R203A apoenzyme at 10 nM was incubated with various amounts of FMN. A double-reciprocal plot of protein fluorescence quenching versus FMN concentration was constructed. From such a plot, the dissociation constant of the binding of the cofactor FMN to the R203A apoenzyme was found to be 0.11 μM. This K_d was very close to the 0.2 μM K_d previously found for the native FRP (*8*).

Reductive Potentials. The standard reduction potential $E^{\circ\prime}$ of R203A was determined by anaerobic titrations with NADH, with phenosafranin as a redox standard. After each NADH addition, the sample was allowed to reach redox equilibrium and the absorption spectrum was recorded (Figure 2A). Values of ΔA_{540} (defined as initial A_{540} minus the A_{540} at each equilibrium state) were used to determine the concentrations of PS_{ox} and PS_{red} at each equilibrium state. $R203A_{ox}$ and $R203A_{red}$ levels were similarly determined from values of ΔA_{465} after the contributions of PS_{ox} were subtracted. Log $[R203A_{ox}]/[R203A_{red}]$ is plotted against log $[PS_{ox}]/[PS_{red}]$, yielding a linear line. On the basis of the ordinate intercept of such a plot and the −252 mV standard reduction potential for PS ($\Delta E^{\circ\prime}_{PS}$), the standard reduction potential of R203A ($\Delta E^{\circ\prime}_{R203A}$) was calculated to be −259 mV according to the rearranged standard Nernst equation in which F is the Faraday constant, R is the gas constant, and T is absolute temperature:

$$\log ([R203A]_{ox}/[R203A_{red}]) = (\Delta E^{\circ\prime}_{PS} - \Delta E^{\circ\prime}_{R203A})\frac{2F}{2.303RT} + \log ([PS_{ox}]/[PS_{red}]) \quad (1)$$

The standard reduction potential for FRP was similarly determined under identical conditions and a value of −254 mV was obtained.

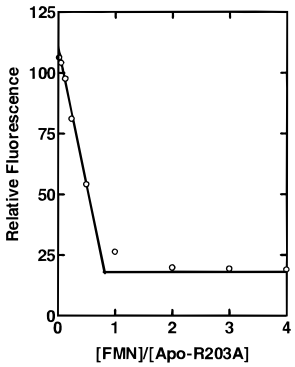

FIGURE 1: Fluorometric titration of FRP apoenzyme with FMN. A constant amount of apoenzyme at 1 μM was titrated with FMN in 0.05 M P_i buffer, pH 7.0. Emission intensities at 330 nm were measured, after 280 nm excitation, and were plotted against molar ratios of FMN/monomeric apoenzyme.

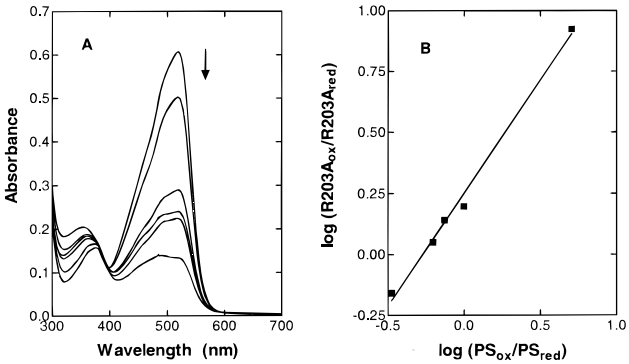

FIGURE 2: Determination of the standard reduction potential of R203A. Aliquots of NADH were added sequentially into 1 mL of 50 mM P_i buffer containing 20 μM phenosafranin, 2 μM benzyl viologen, and 20 μM R203A. Panel A shows the spectral changes in the direction of the arrow with increasing amounts of added NADH. The ratio of $A_{540}/\Delta A_{540}$ gives the value of $[PS_{ox}]/[PS_{red}]$, where ΔA_{540} is the difference of the original absorbance at 540 nm minus the observed A_{540} after the addition of a given amount of NADH. $[R203A_{ox}]/[R203A_{red}]$ was similarly determined by the ratio of $A_{465}/\Delta A_{465}$, where all absorbance readings at 465 nm were those after the subtraction of the contribution by PS_{ox}. The plot of log $[R203A_{ox}]/[R203A_{red}]$ versus log $[PS_{ox}]/[PS_{red}]$ is presented in panel B.

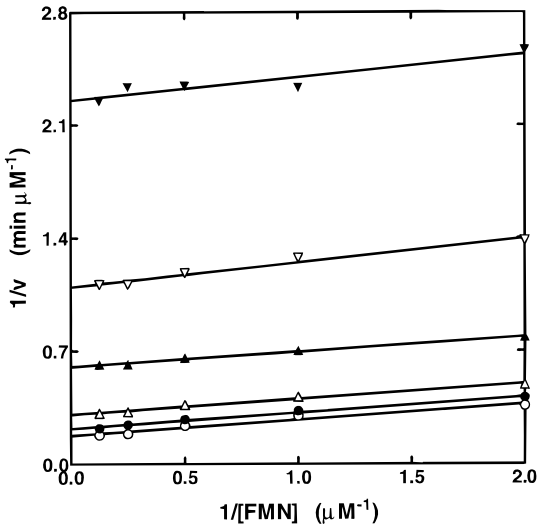

FIGURE 3: Steady-state kinetic analyses of the R203A variant. Initial rates of decreases in A_{340} were measured after 0.01 μM R203A was mixed with designated amounts of FMN and NADPH in 1 mL of 50 mM P_i buffer. The double-reciprocal plots of initial velocity versus FMN concentration at constant levels of NADPH are shown. NADPH concentrations are, from top to bottom, 10, 20, 40, 80, 120, and 160 μM.

Steady-State Kinetic Analyses. The activities of FRP and R203A were determined as a function of FMN concentration at several constant levels of NADPH. The rates of NADPH oxidation were calculated on the basis of initial ΔA_{340}/min and ϵ_{340} of 6.2 mM^{-1} cm^{-1}. Figure 3 shows the double-reciprocal plot of the rate of NADPH oxidation versus FMN concentration for the data obtained with R203A. The pattern of parallel lines indicates that the reaction follows a ping-pong kinetic mechanism similar to that reported earlier (*1*, *15*) and confirmed in this study for the native FRP. The secondary plot of the intercept on the ordinate versus the reciprocal of NADPH concentration from Figure 3 is presented in Figure 4A (●) in comparison with the results obtained similarly with the wild-type FRP (○). On the basis of such a secondary plot, k_{cat} values of 3230 and 4170 min^{-1} were obtained for R203A and FRP, respectively. In contrast to the similar values of k_{cat}, the $K_{m,NADPH}$ of 710 μM for R203A determined from the same secondary plot was much larger than that of 21 μM for FRP. The same sets of data in Figure 3 were reanalyzed for the secondary plot shown in Figure 4B. In this case, R203A was similar to FRP with respect to not only k_{cat} but also $K_{m,FMN}$ (with 5.8 and 6.9 μM for R203A and FRP, respectively).

Binding of NADP$^+$. $NADP^+$ binding by R203A was also compared with that by the wild-type FRP by absorption spectroscopy (Figure 5). When 40 μM FRP was mixed with 0.3 mM $NADP^+$, the binding of $NADP^+$ was readily detected by the changes in the absorption spectrum of the FMN cofactor of FRP. With R203A in place of FRP under otherwise identical conditions, the absorption spectrum of the R203A FMN cofactor did not show any significant changes.

Catalytic Activity with NADH as a Substrate. The wild-type FRP uses NADH at a much lower efficiency than NADPH. When FRP was assayed at a constant level of FMN and increasing concentrations of NADH up to a level still suitable for absorption spectrophotometric measurement, the reaction rates of FRP showed a linear dependence on NADH concentration (Figure 6, ○). Thus, NADH at up to 0.45 mM was still far below the K_m. Such results do not allow the determination of the value of V_{max} or K_m. However, a value of $k_{cat}/K_m = 3 \times 10^5$ M^{-1} min^{-1} can be determined for FRP. The same experiment was repeated with R203A under otherwise identical conditions. Again, the R203A activity showed a linear dependence on NADH concentration, and a value of 4×10^5 M^{-1} min^{-1} for k_{cat}/K_m was obtained (Figure 6, ●).

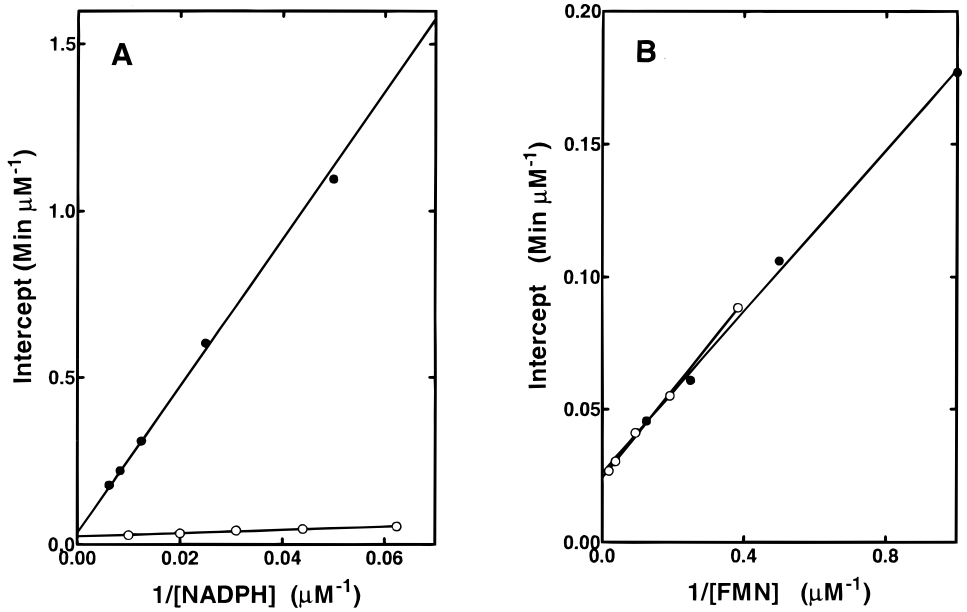

FIGURE 4: Steady-state kinetic analyses of FRP and R203A. On the basis of plots shown in Figure 3 for R203A, the ordinate intercepts are plotted versus the reciprocals of the NADPH concentrations (●, panel A). The same original results in Figure 3 were reanalyzed for double-reciprocal plots of initial velocity versus NADPH concentration at several constant levels of FMN. The ordinate intercepts are also plotted versus the reciprocals of the FMN concentrations (●, panel B) for R203A. The experiments were then repeated with 0.03 μM FRP per assay in place of R203A under otherwise identical conditions. Results were similarly analyzed and shown as the (○) symbols in panels A and B for FRP.

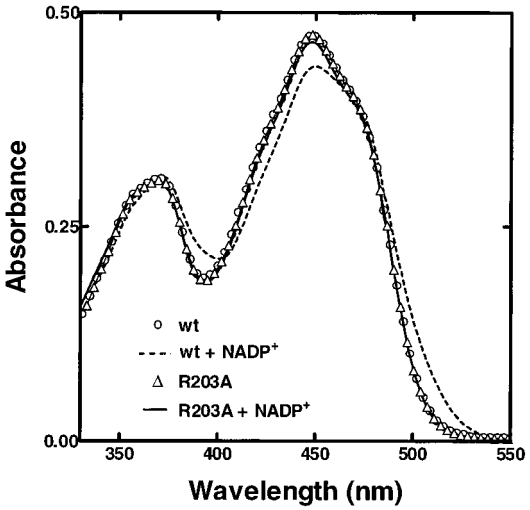

FIGURE 5: Effects of $NADP^+$ on the absorption spectra of FRP and R203A. The absorption spectra were recorded before and after the addition of 0.3 mM $NADP^+$ to 40 μM of either the wild-type FRP or the R203A variant.

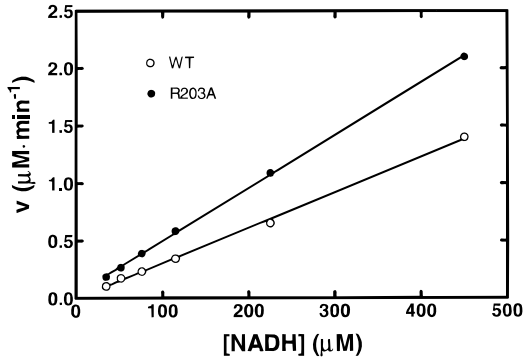

FIGURE 6: Steady-state kinetic analyses of FRP and R203A with NADH as a substrate. Decreases in A_{340} were measured immediately after mixing of 0.16 μM FRP (○) or R203A (●) with 45 μM FMN and various amounts of NADH as designated in 1 mL of 50 mM P_i buffer. Initial velocities (expressed as micromoles per liter per minute for NADH oxidation) were plotted as a function of the corresponding NADH concentrations.

Deuterium Isotope Effect. The activities of FRP and R203A were determined as a function of NADPH or NADPD concentration at a saturating level (50 μM) of FMN. Figure 7 shows the double reciprocal plots of the reaction rate versus the concentration of NADPH (●) or NADPD (○) for FRP (panel B) and R203A (panel A). The ^DV and $^D(V/K)$ were calculated from the intercepts on ordinate and slopes to be 1.7 and 1.4, respectively, for FRP and 3.8 and 4.0, respectively, for R203A.

DISCUSSION

A clue that the Arg203 residue of *V. harveyi* FRP might be important in the specific recognition of NADPH was revealed by a computer modeling of NADPH binding as elaborated above. Such a possible functional role of the Arg203 residue was further supported by other considerations. In addition to FRP, the crystal structures of the *Vibrio fischeri* FRase I (*16*) (or FRG according to our classification) and the *Thermus thermophilus* NADH oxidase (*17*) have also been determined. It has been noted (*9*, *10*, *18*) that while FRP shows significant structural similarities with FRase I

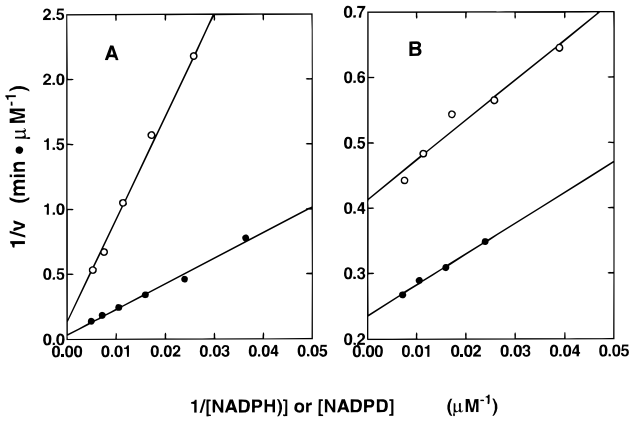

FIGURE 7: Deuterium isotope effects of NADPD on FRP and R203A. The reactions were carried out in 1 mL of 50 mM P_i buffer containing 50 μM FMN, 10 nM R203A or 2.5 nM FRP, and NADPH or NADPD at concentrations as indicated. Initial rates of NADPH (●) or NADPD (○) oxidation were analyzed as a function of NADPH (or NADPD) concentrations as double-reciprocal plots for R203A (panel A) and FRP (panel B).

	191 ↓	203 ↓	220 ↓
FRP	S**YD**QT**M**QA**YY**AS**RTSN**QKLS**TWS**QEVTGK**L**		
NfsA	Q**YDE**QLA**EYY**LT**R**G**SN**N**R**R**DTWSD**HI**R**RT**I**		
SNrA	R**YDE**QLA**EYY**LT**R**G**SN**T**R**R**DTWSD**HI**R**RT**L**		
YWCG_BACSU	T**YD**KTISD**YY**RE**RT**NGK**R**EE**TWSD**QI**L**NFM**		
CHRR_PSESP	A**Y**NDT**M**EA**YY**NN**R**S**SN**RKI**D**N**W**TKQMADF**L**		
YCND_BACSU	A**YDE**Q**M**S**EY**MNK**RT**NGKETRN**WS**QS**I**AS**Y**Y		

FIGURE 8: Comparison of the FRP $residue_{191}$−$residue_{220}$ sequence with homologous sequences. The homologous sequences were obtained by searching the Blast server from National Center for Biotechnology Information (NCBI) against the complete sequence of FRP. The six homologous sequences were further aligned by CLUSTLW, also developed at NCBI. Partial sequences of $residue_{191}$−$residue_{220}$ according to the residue numbers of FRP are shown for *V. harveyi* FRP, NfsA (the *E. coli* major nitroreductase A), SNrA (*Salmonella typhimurium* major nitroreductase), YWCG_BACSU (*Bacillus subtilis* hypothetical 28.3 kDa protein in the QOXD-VPR intergenic region), CHRR_PSESP (*Pseudomonas* sp. Cr(VI) reductase), and YCND_BACSU (*B. subtilis* hypothetical 27.9 kDa protein in the PHRC-GDH intergenic region). The boldface letters indicate identical residues, and the underlined letters refer to similar residues.

and NADH oxidase, the latter two enzymes are substantially more homologous to each other than to FRP. One major structural difference is that the Arg203 residue of the NADPH-preferring FRP is within a disordered $residue_{201}$−$residue_{209}$ loop whereas the *V. fischeri* FRase I/FRG and the *T. thermophilus* NADH oxidase do not discriminate between NADH and NADPH and neither has such a loop. Moreover, the sequence of FRP was used in a search and several homologous proteins were found. The alignment of these homologous sequences corresponding to the FRP $residue_{191}$−$residue_{220}$ peptide is shown in Figure 8. Interestingly, the Arg203 resude is conserved in all of these proteins. Finally, while we did not find any literature information for the pyridine nucleotide specificity for four of these proteins, the *E. coli* nitroreductase NfsA is known to be similar to FRP in its high specificity toward NADPH (*19*). Taking these considerations together, the FRP Arg203 is hypothesized to be critical to the specific recognition of NADPH and this study was initiated to investigate such a working hypothesis.

The crystal structures of FRP show no direct participation of the Arg203 in the FMN cofactor binding (*9*, *10*). It was expected that the mutation of Arg203 to an alanine residue would not adversely affect the FMN cofactor binding. Indeed, the R203A variant was similar to the wild-type FRP with respect to the single site per reductase monomer (Figure 1) and the K_d for the FMN cofactor binding. Moreover, the −259 mV standard reduction potential of R203A (Figure 2) was also found to be essentially the same as that for the wild-type FRP.

The crystal structures of FRP, however, do not reveal any direct information regarding the nature of the binding of NADPH or the flavin substrate. The ability to recognize and utilize these two substrates by the R203A variant was compared with that of the wild-type FRP by an examination of their steady-state kinetic characteristics. Similar to the wild-type FRP, R203A displayed a ping-pong kinetic pattern (Figure 3). In comparison with FRP, the mutation of Arg203 to alanine resulted in only minor changes in V_{max} and the K_m for the FMN substrate (Figure 4B). Therefore, the Arg203 residue appeared not to have any major functional role in the binding and utilization of the FMN substrate. However, the K_m of the R203A variant for NADPH (710 μM) was much higher than that (21 μM) for FRP (Figure 4A). Such a finding is quite consistent with the proposed functional role of Arg203 in NADPH recognition and binding.

The wild-type FRP was also able to bind $NADP^+$ as shown by the perturbation of the FMN cofactor absorption spectrum upon addition of $NADP^+$ (Figure 5). However, no significant spectral perturbation was observed upon addition of $NADP^+$ to the R203A variant (Figure 5). This could be due to a lack of significant binding of $NADP^+$ (at 0.3 mM) by the R203A. Assuming <5% of R203A was bound by $NADP^+$ under conditions described for Figure 5, the K_d for $NADP^+$ binding by R203A is estimated to be >5.7 mM, a value substantially higher than the 0.25 mM K_d for $NADP^+$ binding by the wild-type FRP (*11*). Our results cannot exclude the possibility that $NADP^+$ can be significantly bound by R203A but the binding did not result in any noticeable absorption spectral perturbation of the mutated reductase. Even in such a case, our spectroscopic data indicate that the nature of $NADP^+$ binding was significantly different between the wild-type FRP and R203A. In either case, these observations further support the proposed critical role of Arg203 in the recognition of the 2′-phosphate attached to the adenosine moiety of NADPH/$NADP^+$.

If Arg203 is critical to the discrimination between NADPH and NADH by FRP, the mutation of Arg203 to an alanine should not have any marked effect on the ability of the reductase to utilize NADH as a substrate. For both the wild-type FRP and R203A, their K_m values for NADH were apparently much higher than the NADH concentrations used for results shown in Figure 6. However, these results allow the determination of $k_{cat}/K_{m,NADH}$ values of 3×10^5 and 4×10^5 M^{-1} min^{-1} for FRP and R203A, respectively. The close similarity of FRP and R203A in their $k_{cat}/K_{m,NADH}$ is quite distinct from the marked difference in values of $k_{cat}/K_{m,NADPH}$ for FRP (1990×10^5 M^{-1} min^{-1}) and R203A (46×10^5 M^{-1} min^{-1}) determined from results shown in Figure 4.

Deuterium isotope effects of (4*R*)-[4-^{2}H]NADPH (NADPD) were tested to further elucidate the functional role of Arg203. The relatively small ^DV and $^D(V/K)$ effects of 1.7 and 1.4, respectively, for the native FRP were increased to 3.8 and 4.0, respectively, for R203A (Figure 7). Following the general scheme

$$E + S \underset{k_2}{\overset{k_1}{\rightleftharpoons}} ES \underset{k_4}{\overset{k_3}{\rightleftharpoons}} EP \xrightarrow{k_5} E + P$$

where S is NADPH (or NADPD), P is $NADP^+$, and k_3 (= the reduction of FRP FMN cofactor by NADPH or NADPD) and k_4 are the isotope-sensitive steps, the isotope effects can be expressed as

$$^DV = \frac{^Dk_3 + (k_{3H}/k_5) + (k_{4H}/k_5)^DK_{eq}}{1 + (k_{3H}/k_5) + (k_{4H}/k_5)} \quad (2)$$

$$^D(V/K) = \frac{^Dk_3 + (k_{3H}/k_2) + (k_{4H}/k_5)^DK_{eq}}{1 + (k_{3H}/k_2) + (k_{4H}/k_5)} \quad (3)$$

In comparison with FRP, the dissociation of NADPH (k_2) and $NADP^+$ (k_5) of R203A must both become substantially faster relative to k_3 and k_4. Thus, the mutation of Arg203 to alanine markedly reduced the affinity of NADPH or $NADP^+$ binding.

Among the three known species of flavin reductases in luminous bacteria, the FRP exhibits a uniquely high degree of specificity toward NADPH. In the present study, functional consequences of the mutation of the conserved Arg203 residue of FRP to an alanine were examined with respect to FMN and pyridine nucleotide binding, reduction potential of the bound flavin cofactor, steady-state kinetics, and deuterium isotope effects. Results from all of these studies fully support the hypothesis that Arg203 is critical to the specific recognition and utilization of NADPH by FRP. Since this Arg203 residue is highly conserved (Figure 8), the present finding suggests that this residue may have a similar functional role in other homologous proteins.

A number of pyridine nucleotide-dependent enzymes have been examined with respect to the molecular basis for their cofactor specificity toward NAD(H) or NADP(H). A generality has emerged from these studies. For many NAD(H)-specific enzymes [such as several species of dihydrolipoamide dehydrogenase (*20*), horse liver (*21*) and *Drosophila* (*22*) alcohol dehydrogenases, *Lactobacollus delbrueckii* (subspecies *bulgaricus*) D-lactate dehydrogenase (*23*), *Bacillus stearothermophilus* L-lactate dehydrogenase (*24*) and glyceraldehyde-3-phosphate dehydrogenase (*25*), and *Pseudomonas mevalonii* 3-hydroxy-3-methylglutaryl-CoA reductase (*26*)], their high selectivity for NAD(H) is related to the interaction of an aspartate residue with the 2′-hydroxy group of the cofactor adenosine moiety. On the other hand, a number of enzymes have been shown to involve the interaction between a lysine residue [such as *Pichia stipitis* xylose reductase (*27*)) or, especially, an arginine residue (such as several species of glutathione reductases (*20*, *28*), *Escherichia coli* isocitrate dehydrogenase (*29*), mouse lung carbonyl reductase (*30*), and *Lactococcus lactis* 6-phosphogluconate dehydrogenase (*31*)] and the 2′-phosphate of NADP(H) as a determinant for their cofactor selectivity. Consistent with such a general pattern, we have now identified Arg203 as a critical residue in the recognition and binding of NADPH by *V. harveyi* FRP. The protein fold of

FRP is distinct from that of the other NADP(H)-preferring enzymes mentioned above (*9*, *10*). Therefore, the present work provides an example from a new structural class of enzymes for the essential role of arginine in enzyme specificity toward NADP(H).

REFERENCES

1. Lei, B., and Tu, S.-C. (1998) *Biochemistry 37*, 14623−14629.
2. Gerlo, E., and Charlier, J. (1975) *Eur. J. Biochem. 57*, 461−467.
3. Jablonski, E., and DeLuca, M. (1977) *Biochemistry 16*, 2932−2936.
4. Michaliszyn, G. A., Wing, S. S., and Meighen, E. A. (1977) *J. Biol. Chem. 252*, 7495−7499.
5. Watanabe, H., and Hastings, J. W. (1982) *Mol. Cell. Biochem. 44*, 181−187.
6. Lei, B., Liu, M., Huang, S., and Tu, S.-C. (1994) *J. Bacteriol. 176*, 3552−3558.
7. Duane, W., and Hastings, J. W. (1975) *Mol. Cell. Biochem. 6*, 53−64.
8. Liu, M., Lei, B., Ding, Q., Lee, J. C., and Tu, S.-C. (1997) *Arch. Biochem. Biophys. 337*, 89−95.
9. Tanner, J. J., Lei, B., Tu, S.-C., and Krause, K. L. (1996) *Biochemistry 35*, 13531−13539.
10. Tanner, J. J., Tu, S.-C., Barbour, L. J., Barnes, C. L., and Krause, K. L. (1999) *Protein Sci. 8*, 1725−1732.
11. Tu, S.-C., Lei, B., Yu, Y., and Liu, M. (1997) in *Flavins and Flavoprotein* (Stevenson, K. J., Massey, V., and Williams, C. H., Jr., Eds.) pp 357−366, University of Calgary Press, Calgary, Alberta, Canada.
12. Studier, F. W., and Moffatt, B. A. (1986) *J. Mol. Biol. 189*, 113−130.
13. Sem, D. S., and Kasper, C. B. (1992) *Biochemistry 31*, 3391−3398.
14. Williams, C. H., Jr., Arscott, L. D., Matthews, R. G., Thorpe, C., and Wilkinson, K. D. (1979) *Methods Enzymol. 62*, 185−198.
15. Jablonski, E., and DeLuca, M. (1978) *Biochemistry 17*, 672−678.
16. Koike, H., Sasaki, H., Kobori, T., Zenno, S., Saigo, K., Murphy, M. E., Adman, E. T., and Tanokura, M. (1998) *J. Mol. Biol. 280*, 259−273.
17. Hecht, H. J., Erdmann, H., Park, H. J., Sprinzl, M., and Schmid, R. D. (1995) *Nat. Struct. Biol. 2*, 1109−1114.
18. Koike, H., Sasaki, H., Tanokura, M., Zenno, S., and Saigo, K. (1996) *J. Struct. Biol. 117*, 70−72.
19. Zenno, S., Kobori, T., Tanokura, M., and Saigo, K. (1998) *J. Bacteriol. 180*, 422−425.
20. Scrutton, N. S., Berry, A., and Perham, R. N. (1990) *Nature 343*, 38−43.
21. Fan, F., Lorenzen, J. A., and Plapp, B. V. (1991) *Biochemistry 30*, 6397−401.
22. Chen, Z., Lee, W. R., and Chang, S. H. (1991) *Eur. J. Biochem. 202*, 263−7.
23. Bernard, N., Johnsen, K., Holbrook, J. J., and Delcour, J. (1995) *Biochem. Biophys. Res. Commun. 208*, 895−900.
24. Holmberg, N., Ryde, U., and Bulow, L. (1999) *Protein Eng. 12*, 851−6.
25. Didierjean, C., Rahuel-Clermont, S., Vitoux, B., Dideberg, O., Branlant, G., and Aubry, A. (1997) *J. Mol. Biol. 268*, 739−59.
26. Friesen, J. A., Lawrence, C. M., Stauffacher, C. V., and Rodwell, V. W. (1996) *Biochemistry 35*, 11945−50.
27. Kostrzynska, M., Sopher, C. R., and Lee, H. (1998) *FEMS Microbiol. Lett. 159*, 107−12.
28. Pai, E. F., Karplus, P. A., and Schulz, G. E. (1988) *Biochemistry 27*, 4465−74.
29. Hurley, J. H., Chen, R., and Dean, A. M. (1996) *Biochemistry 35*, 5670−8.
30. Tanaka, N., Nonaka, T., Nakanishi, M., Deyashiki, Y., Hara, A., and Mitsui, Y. (1996) *Structure 4*, 33−45.
31. Tetaud, E., Hanau, S., Wells, J. M., Le Page, R. W., Adams, M. J., Arkison, S., and Barrett, M. P. (1999) *Biochem. J. 338*, 55−60.

BI0003745